Comparison of time–delayed feedback schemes for spatio–temporal control of chaos in a reaction–diffusion system with global coupling

O. Beck[a)], A. Amann[a)], E. Schöll[a)], J. E. S. Socolar[b)], and W. Just[c),a)] * †
[a)] *Institut für Theoretische Physik, TU Berlin, Hardenbergstr. 36, D–10623 Berlin, Germany*
[b)] *Department of Physics, Duke University, Durham, NC 27708, USA*
[c)] *Institut für Physik, TU Chemnitz, D–09107 Chemnitz, Germany*
(May 5, 2002)

Time–delayed feedback control for stabilising time periodic spatial patterns is investigated in a generic reaction–diffusion system with global coupling. We focus on the case of low-dimensional chaos where unstable patterns admit only a single unstable mode. Spatial degrees of freedom are taken into account to define different control schemes. The efficiency of these schemes is discussed, where control forces are motivated by physical requirements as well as by the possibility of obtaining analytically exact results. We find that control schemes which contain the full feedback of the inhibitor variable may finally destroy the control performance. Thus schemes which omit the inhibitor might be more efficient. Our numerical findings are explained in terms of Floquet spectra and compared with analytical solutions of particular coupling schemes.

PACS numbers: 05.45.Gg, 05.45.Jn, 02.30.Ks

I. INTRODUCTION

Control of complex chaotic dynamics has become one of the central issues in applied nonlinear science over the last decade (cf. [1]). Control theory is of course a well established discipline in engineering and applied mathematical sciences for almost half a century (cf. e.g. [2]), but its application often requires either some information about the structure of the system or some data processing. The new aspect of chaos control is the emphasis of noninvasive control methods together with the observation that chaos supplies a huge number of unstable states that can be stabilised with tiny control power [3]. A particularly simple and efficient scheme uses time–delayed signals to generate control forces for stabilising time periodic states [4] (time–delay autosynchronisation or "Pyragas method"). It is simple to implement, quite robust, and has been applied successfully in real experiments [5,6]. But the performance of the control method cannot be understood in a straightforward way. Analytical insight into this scheme has been gained just recently [7,8].

An important ingredient in any control method is the choice of the coupling of control forces to the dynamical degrees of freedom. Unfortunately this question has not been addressed systematically for time–delayed feedback methods. Only a few preliminary results are available in the literature [9,10]. Here we will discuss this topic in the context of a reaction–diffusion model with a global constraint. Such models are relevant in different fields of physics and chemistry, e.g. for the dynamics of semiconductor devices (cf. [11] for a recent review) or in electrochemistry [12]. Thus we expect that our investigations show generic features which are of use in quite different fields of science.

The model we are dealing with was originally derived for charge transport in a layered semiconductor system such as the heterostructure hot electron diode [13]. The resulting model equations in nondimensional units read

$$\begin{aligned} \partial_t u(t) &= \alpha[j_0 - (u - \langle a \rangle)] - KF_u(t) \\ \partial_t a(x,t) &= f(u-a) - Ta + \partial_x^2 a - KF_a(x,t) \quad . \end{aligned} \tag{1}$$

Here $u(t)$ is the inhibitor and $a(x,t)$ the activator variable. In the semiconductor context $u(t)$ denotes the voltage drop across the device and $a(x,t)$ is an internal degree of freedom, e.g. an interface charge density. The local current density in the device is $j(x,t) \equiv u(t) - a(x,t)$, and j_0 is the externally applied current which acts as a control parameter. The one–dimensional spatial coordinate x corresponds to the direction transverse to the current. We consider a system of width L with Neumann boundary conditions $\partial_x a = 0$ at $x = 0, L$ corresponding to no charge transfer through the

* e–mail: wolfram.just@physik.tu-chemnitz.de
† permanent address: School of Mathematical Sciences, Queen Mary / Univ. of London, Mile End Road, London E1 4NS, UK

lateral boundaries. T denotes the tunnelling rate through the collector layer. The relaxation rate α is determined by the internal and external capacitance. The global coupling represented by

$$\langle a \rangle(t) = \frac{1}{L} \int_0^L a(x,t)\, dx. \tag{2}$$

arises from the application of Kirchhoff's law to the circuit in which the device is operated [11]. The nonlinear part of the transport equation, giving rise to an S–shaped local current density vs. field characteristic, is canonically modelled by a simple Lorentzian of the form

$$f(j) = j/[j^2 + 1] \quad . \tag{3}$$

Eqs.(1) contain control forces F_a and F_u for stabilising time periodic patterns. Details of different choices for these forces and different control schemes are discussed below (cf. table I). The strength of control terms is proportional to the control amplitude K, which gives one important parameter of each control scheme. In the semiconductor context these forces can be implemented by appropriate electronic circuits [10].

The dynamics of the free system, i.e. $K = 0$, is very well understood [14–16]. For our purpose it is important that the model develops temporally chaotic and spatially nonuniform states (spatio–temporal spiking, cf. Figure 1) in appropriate parameter regimes. For any value of L the system, due to the global coupling, allows only single spikes at the boundary of the spatial domain [17]. These are associated with low-dimensional chaos where only one unstable Lyapunov exponent exists [14]. Throughout this paper we focus on the special choice $\alpha = 0.035$, $T = 0.05$, $L = 40$ and $j_0 = 1.262$. In the semiconductor context the time and length scales of our dimensionless variables are typically given by picoseconds and micrometers, respectively.

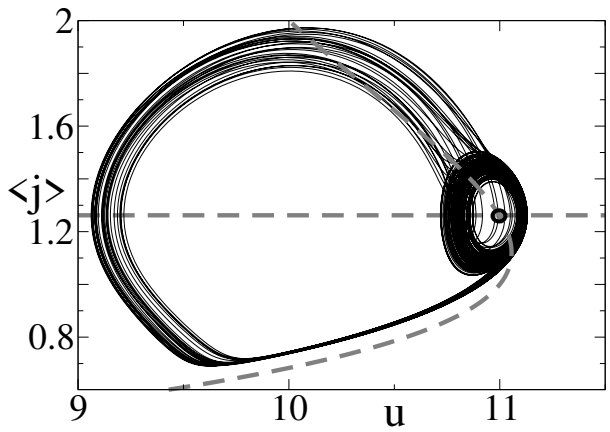

FIG. 1. Projected phase portrait of the uncontrolled system in the $(\langle j \rangle, u)$ plane. The null-isoclines of the uniform system are plotted as dashed lines. The uniform fixed point at $u = 11.0$, $\langle j \rangle = 1.27$ is indicated by a dot, and the chaotic spatio–temporal attractor is represented by its projected trajectory.

We are concerned with controlling unstable time periodic patterns $u_p(t) = u_p(t+\tau)$, $a_p(x,t) = a_p(x,t+\tau)$ which are embedded in a chaotic attractor. For that purpose we apply control forces F_a and F_u which are derived from time–delayed differences of the voltage and the charge density. For example we may choose $F_u = F_{\rm vf}$ with the voltage feedback force

$$F_{\rm vf}(t) = u(t) - u(t-\tau) + RF_{\rm vf}(t-\tau) \quad . \tag{4}$$

The last contribution, involving the filter parameter $|R| < 1$ corresponds to an improvement by multiple time–delays proposed in [18] (extended time–delay autosynchronisation), whereas the original scheme based on a simple time–delayed difference corresponds to the choice $R = 0$. For consideration of the case $R > 1$, see [19].

Here we concentrate on the question how the coupling of the control forces to the internal degrees of freedom influences the performance of the control. For our model we consider two different choices for the control force F_a. On the one hand we use a force which is based on the local charge density according to

$$F_{\rm loc}(x,t) = a(x,t) - a(x,t-\tau) + RF_{\rm loc}(x,t-\tau) \quad . \tag{5}$$

whereas on the other hand we propose a construction which is only based on its spatial average

$$F_{\mathrm{glo}}(t) = \langle a \rangle(t) - \langle a \rangle(t-\tau) + R F_{\mathrm{glo}}(t-\tau) \quad . \tag{6}$$

We call the choice $F_a = F_{\mathrm{loc}}$ a *local* control scheme in contrast to the *global* control scheme $F_a = F_{\mathrm{glo}}$ which requires only the global average and does not depend explicitly on the spatial variable. The second option has considerable experimental advantages since the spatial average can be obtained by a simple measurement of the total current $\langle j \rangle = u - \langle a \rangle$.

Finally we distinguish between control schemes which use no voltage feedback $F_u \equiv 0$, full voltage feedback $F_u = F_{\mathrm{vf}}$, or even partial voltage feedback $F_u = \varepsilon F_{\mathrm{vf}}$ with $0 < \varepsilon < 1$. The different schemes discussed in the following sections are summarised in table I.

Type of control	F_a	F_u	Section
diagonal control	F_{loc}	F_{vf}	II
local control	F_{loc}	0	III
global control without voltage feedback	F_{glo}	0	III
global control with voltage feedback	F_{glo}	F_{vf}	IV
global control with partial voltage feedback	F_{glo}	$\varepsilon F_{\mathrm{vf}}$	IV

TABLE I. Overview of different control schemes with the corresponding choices of F_a and F_u

II. DIAGONAL CONTROL

In general the analysis of the control performance of time–delayed feedback methods results in differential–difference equations which are hard to tackle and analytical results on the linear stability analysis have been obtained only recently [7–9]. Stability of the orbit is governed by eigenmodes and the corresponding complex valued growth rates Λ (Floquet exponents). The eigenvalue equation which determines these exponents can be cast into the form [20]

$$\Lambda = \Gamma\left(K \frac{1-\exp(-\Lambda\tau)}{1-R\exp(-\Lambda\tau)}\right) \quad . \tag{7}$$

The right hand side contains a function $\Gamma(\kappa)$ which is determined by the linear stability of the free orbit and the coupling scheme of the control forces. The argument of Γ in eq.(7) arises via a Laplace transform of the control forces (cf. e.g. eq.(4)).

In general it is difficult to evaluate eq.(7) quantitatively, since the explicit form of the function $\Gamma(\kappa)$ is unknown. There exists, however, a simple case (which we call *diagonal* control) where the right hand side is given by $\Gamma(\kappa) = \lambda - \kappa$ [7]. Here λ denotes any of the Floquet exponents of the uncontrolled orbit. In our context the diagonal control scheme corresponds to the choice $F_a = F_{\mathrm{loc}}$ and $F_u = F_{\mathrm{vf}}$. It is a straightforward extension to a spatially extended system of an identity matrix for the control of discrete systems of ordinary differential equations (cf. [9]). In such schemes, every dynamical variable is monitored and feedback is applied to each one based only on its own behavior. Moreover, the feedback gain is the same for every variable. The diagonal scheme is amenable to analytical treatment, which makes it useful as a reference point, to which other control schemes may be compared. Thus for the diagonal coupling scheme eq.(7) reduces to the exact equation [21]

$$\Lambda = \lambda - K \frac{1-\exp(-\Lambda\tau)}{1-R\exp(-\Lambda\tau)} \quad . \tag{8}$$

Successful control corresponds to those control parameter values (K, R) for which eq.(8) yields Floquet exponents Λ with negative real part only.

For the numerical simulations we concentrate on the unstable periodic orbit with period $\tau = 984.85$, which has only one unstable Floquet mode. The corresponding Floquet exponent is $\lambda\tau = 0.490 + i\pi$. We implement the diagonal control scheme for our model (1) using numerical integration with an Euler scheme of stepsize $\Delta t = 0.025$. Spatial degrees of freedom are modelled on a lattice with spatial resolution $\Delta x = L/25$ and the derivative is evaluated up to first order. We have also performed simulations with different step sizes to check that our results, in particular the control domains, are robust against the choice of the step size. Furthermore, the numerical results are in accordance with analytical expressions, where available (cf. Figure 2). As a criterion for successful control we require control

forces to be less than 10^{-4} in amplitude. In order to avoid any complications caused by transient behaviour or by multistability we usually choose initial conditions in the vicinity of the unstable orbit.

In Figure 2 the regime of successful control in the K–R parameter plane is depicted. The control domain has its typical triangular shape bounded by a flip instability ($\mathrm{Re}\Lambda = 0, \mathrm{Im}\Lambda\tau = \pi$) to its left and by a Hopf bifurcation to its right. Inclusion of the filter parameter R increases the range of K over which control is achieved. From eq. (8) it follows that the left boundary (flip instability) is given by the straight line

$$R = \frac{2}{\mathrm{Re}\lambda}K - 1. \tag{9}$$

We observe that the numerical result fits very well with the analytical prediction. The deviations from the right boundary for larger R are numerical artefacts resulting from the very small positive real part of the largest Floquet exponent. Note that the precise location of the control domain, in particular its tip depends on the value of the Floquet exponents λ of the uncontrolled orbit. In particular the orbit of the uncontrolled system must satisfy the constraint $\mathrm{Re}\lambda\tau \leq 2(1+R)/(1-R)$ in order that control works successfully [20].

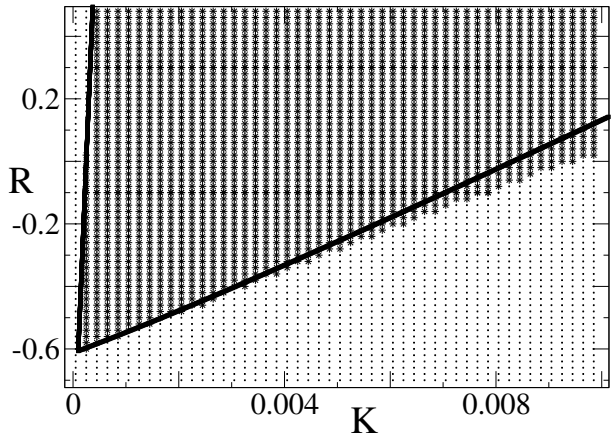

FIG. 2. Control domains in the K–R parameter plane for the unstable periodic orbit with period $\tau = 984.85$. $*$ successful control in the numerical simulation, $\cdot$ no control, lines: analytical result according to eq.(8).

To confirm the bifurcations at the boundaries we consider the Floquet spectrum of the orbit subjected to control. We use a Benettin algorithm [22] for numerical computation of the Floquet exponents. Such an algorithm can be applied easily to obtain the leading part of the eigenvalue spectrum, since one just requires the forward integration of the full system (1) and successive reorthogonalisation. The algorithm yields the real parts of the exponents, $\mathrm{Re}\Lambda$, since it detects the expansion in phase space but ignores the torsion. Thus complex conjugate exponents show up as doubly degenerate pairs. We always obtain a Goldstone mode, $\Lambda = 0$, since we are dealing with an autonomous model. Finally the algorithm shows a numerical hybridisation phenomenon if eigenbranches cross. Such an artefact can be reduced by increasing the integration time and it has to be ignored on interpreting the eigenvalue spectra.

For the diagonal control scheme we have calculated the five Floquet exponents with the largest real part in dependence on K for fixed $R = 0$ (Figure3). The largest nontrivial exponent decreases with increasing K and collides at negative values with a branch coming from negative infinity. As a result a complex conjugate pair develops and real parts increase again. The real part of the exponent finally crosses the zero axis giving rise to a Hopf bifurcation. Our numerical simulations are in agreement with the analytical result according to eq.(8). Note that for the diagonal scheme no other modes interfere with the leading branch [21].

III. CONTROL SCHEMES WITHOUT VOLTAGE FEEDBACK

Let us now concentrate on control schemes without voltage feedback, i.e. on schemes which are solely based on the forces (5) or (6). In particular we will discuss the local control scheme $F_a = F_{\mathrm{loc}}$ and the global scheme without voltage feedback, $F_a = F_{\mathrm{glo}}$. For our numerical simulations we focus again on the unstable orbit with period $\tau = 984.85$ which was already used in the previous section.

We will compare our simulations to analytical results of the eigenvalue equation (7). For small κ a linear approximation can be used: $\Gamma[\kappa] = \lambda + \chi\kappa$ with a constant χ. We refer the reader to [21] for more details concerning this

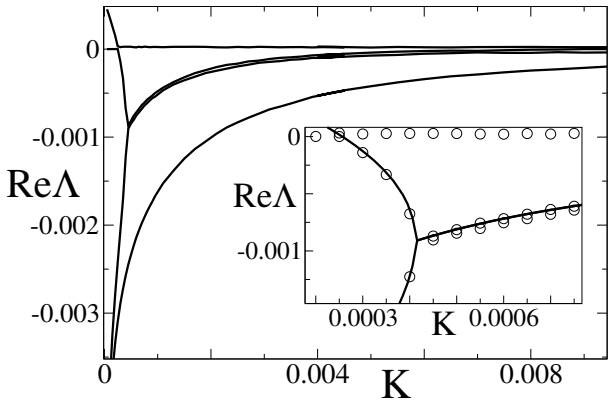

FIG. 3. Leading part of the Floquet spectrum for diagonal control in dependence on K ($R = 0$): from numerical simulation. The inset shows the analytical result according to eq.(8) (lines) vs. numerical data (circles).

assumption. Then the control performance is approximately governed by

$$\Lambda = \lambda + \chi K \frac{1 - \exp(-\Lambda\tau)}{1 - R\exp(-\Lambda\tau)} \quad . \tag{10}$$

The new parameter χ, which is real valued in the case of flip orbits (i.e. $\mathrm{Im}\lambda\tau = \pi$) takes all the details of the control scheme into account.

The results for the control domain in the K–R parameter plane are summarised in Figure 4. Control domains for both schemes look similar in shape, although the domain for the local scheme is shifted slightly towards lower control amplitudes. The left–hand border of the control domain corresponding to a flip instability is very well modelled by the analytical formula (10) with an appropriate choice of the parameter χ. That is not surprising since even the exact eigenvalue equation (7) predicts that the boundary is a straight line: $i\pi/\tau = \Gamma(2K/(1+R))$, hence the argument of Γ is constant and $R + 1 \sim 2K$. The lower right–hand boundary of the control domain does not coincide very well with the analytical expression, a feature already known in low–dimensional dynamical systems. The shape of this boundary depends on details of the system. Most remarkably the domains do not extend to large R values. There exists an upper right–hand cutoff which prevents control beyond the boundary C (Figure 4b). Thus, increasing R does not necessarily increase the control performance[1].

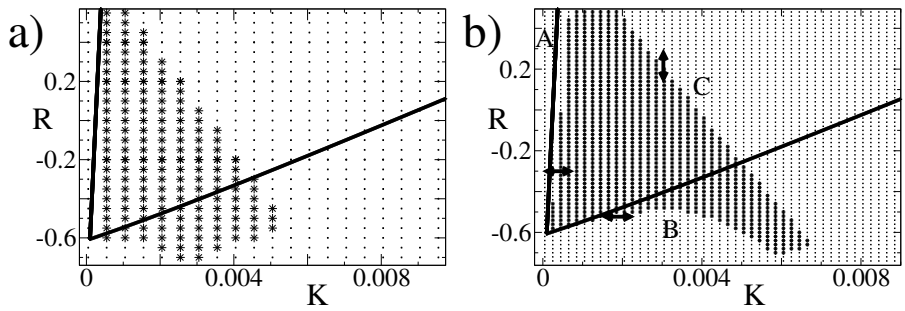

FIG. 4. Control domains for (a) the local and (b) global control scheme without voltage feedback. $*$ domain of control, $\cdot$ no control, lines: analytical result of eq.(10) with $\mathrm{Re}\lambda\tau = 0.490$, $\chi = -1$. Double arrows indicate parameter settings used for the Fourier spectra in Figure 5.

In order to understand the control domains in more detail we will discuss the instability mechanisms which generate the control boundaries. Since both methods generate qualitatively similar control domains we restrict the discussion

[1]We note the existence of a fourth boundary, at the lower right in Figure 4, that has not yet been analyzed in detail.

to the experimentally more relevant global scheme without voltage feedback. Let us first take a look at the Fourier spectra (cf. Figure 5) of the total current $\langle j \rangle$ in the vicinity of the three qualitatively different control boundaries. At the left–hand boundary (A) a peak at half the fundamental frequency develops, which indicates a flip instability (period doubling) in accordance with the theoretical considerations of the previous paragraph. At the lower right–hand boundary (B) sideband frequencies emerge while crossing the control boundary. Although the theoretical prediction of the boundary fails quantitatively, the instability mechanism is in accordance with the Hopf scenario described in Section II. Finally we observe at the upper right–hand boundary (C) a slight shift in the spectrum. In addition the instability is accompanied by strong hysteresis when sweeping the control parameters accross the control boundary (Figure 6). Thus the upper right–hand control boundary is generated by a subcritical bifurcation. The periodic state which appears beyond the threshold is generated by the control loop and does not correspond to an unstable orbit of the free system. In fact it coexists with the proper periodic orbit within the control domain.

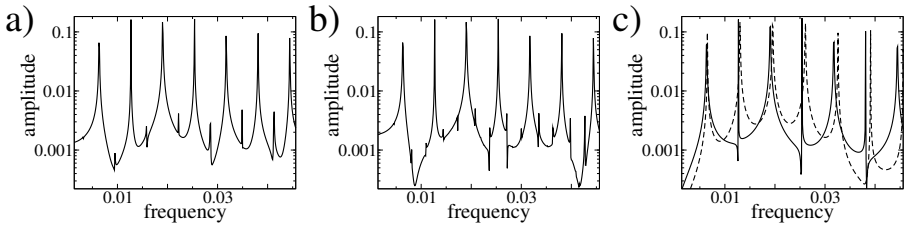

FIG. 5. Fourier spectrum of the total current $\langle j \rangle(t) = u - \langle a \rangle$ for global control without voltage control (a) at the left–hand boundary A ($K = 0.000318$, $R = -0.3$), (b) at the lower right–hand boundary B ($K = 0.0018$, $R = -0.52$), and (c) at the upper right–hand boundary C ($K = 0.003$, $R = 0.216$) (cf. Figure 4b). The dashed line indicates the spectrum of the periodic orbit in the control domain.

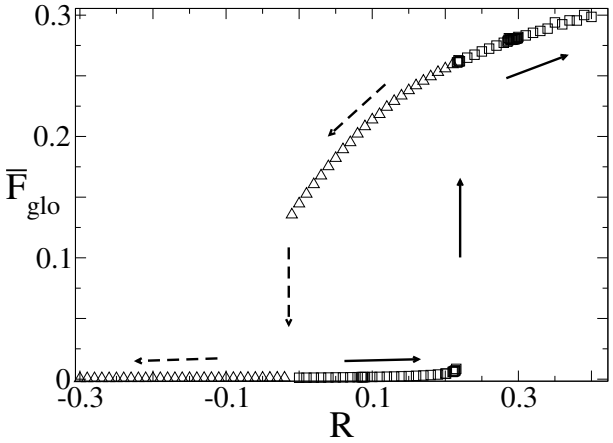

FIG. 6. Temporal average of the control force when sweeping across the upper right–hand control boundary at $K = 0.003$ (line C in Figure 4b).

To uncover the nature of the subcritical bifurcation which constitutes the upper right–hand control boundary we have evaluated the Floquet spectrum too (cf. Figure 7). The spectrum shows a slightly more complicated structure compared to the result of the simple analytical formula (10), which is rigorously valid for diagonal control. One still observes a flip instability at the lower threshold and the typical butterfly shape of the leading eigenvalue branch. But now a real Floquet multiplier $\exp(\Lambda\tau)$ with $\mathrm{Im}\Lambda = \pi/\tau$ and $\mathrm{Re}\Lambda$ coming from $\ln|R|$ crosses the leading complex branch near $K \approx 0.0035$ and takes over the dominant role. It finally yields an upper control threshold ($\mathrm{Re}\Lambda = 0$) at $K \approx 0.0045$, thus giving rise to a subcritical flip instability.

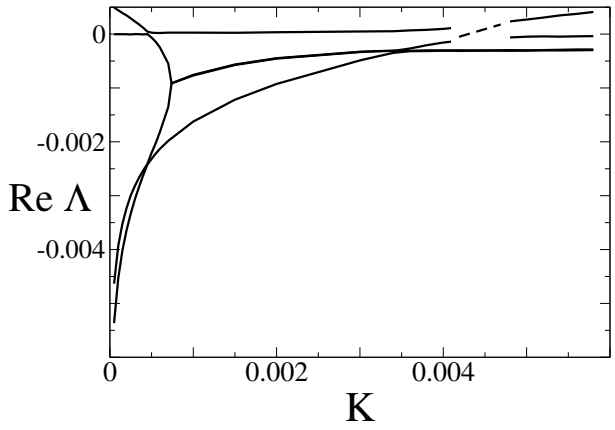

FIG. 7. Leading part of the Floquet spectrum for global control without voltage feedback for $R = 0$. The dashed line interpolates the regime where the numerical accuracy is insufficient due to very small $|\mathrm{Re}\Lambda|$.

IV. GLOBAL CONTROL WITH PARTIAL VOLTAGE FEEDBACK

Control domains for local and global schemes without voltage feedback look similar in shape. But their size is reduced, compared to diagonal control, by an additional subcritical bifurcation limiting the control for large filter parameter R. In fact by varying the current j_0 these domains may shrink and finally they even may vanish. Thus the upper control boundary has a dramatic effect on the control performance. If we include voltage feedback the local scheme becomes the diagonal coupling scheme which is very efficient. A naive guess would expect similar features to happen if the voltage feedback F_{vf} according to (4) is included into the global coupling scheme. Surprisingly the global control scheme with voltage feedback does not work at all, and one hardly finds orbits which can be stabilised with such a scheme. The corresponding Floquet spectrum displays a branch with entirely positive real part, so that stabilisation is never achieved (cf. Figure 8a).

However, if we reduce the relative strength of the voltage feedback, i.e. if we introduce a parameter ε in $F_u = \varepsilon F_{\mathrm{vf}}$ and decrease its value continuously, then the unstable branch moves downwards. At $\varepsilon \approx 0.6$ a region develops where all exponents are negative. A rather large control interval develops at $\varepsilon = 0.4$ as displayed in Figure 8b. The whole structure of the spectrum now resembles to some extent the purely diagonal control scheme (cf. Figure 3). Lowering ε further the spectrum then finally transforms to the form of the global control without voltage feedback (cf. Figure 7). Thus we expect that an optimal feedback ratio for ε can be determined such that control domains become maximal. A full voltage feedback with $\varepsilon = 1$ results in an overshoot and destroys the control performance completely.

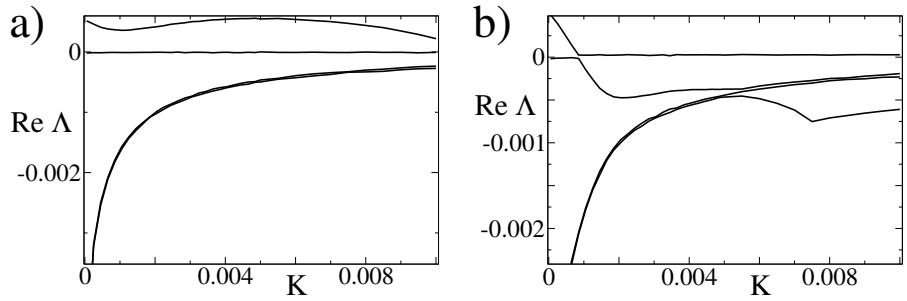

FIG. 8. Floquet spectra for global control with partial voltage feedback for the periodic orbit with period $\tau = 984.85$ for $R = 0$. (a) $\varepsilon = 0.7$, (b) $\varepsilon = 0.4$.

V. CONCLUSION

We have compared different coupling schemes for time–delayed feedback control of spatio-temporal patterns with a single unstable eigenmode. For classical control techniques, such a comparison is one of the central issues of modern control theory and there exists a detailed theory of the control performance. Unfortunately little is known for time–delayed feedback methods, although such methods are easily applicable for the stabilisation of time periodic patterns.

Our investigations have shown that a naive extrapolation of the control performance from the analytically solvable case of diagonal control fails. Although local and global coupling without voltage feedback behave similarly the inclusion of voltage feedback results in completely different control performances. A partial voltage feedback with a weight factor of less than one enhances the control performance.

In addition we observe that Floquet branches which are not present in the system without time–delayed feedback may impose additional limits to the control domains (cf. also [21]). In our case such branches are responsible for subcritical bifurcations and strong hysteresis. In particular the performance of extended time-delay autosynchronization may decline if the filter parameter R is increased. The details of the Floquet spectrum, however, depend on the particular system and the orbit under consideration.

So far there exists no complete and systematic treatment of the effect of different coupling schemes for time–delayed feedback control. Even for the simple case of stabilisation of (time independent) fixed points such a problem requires the analysis of transcendental equations [23]. The situation is even worse if time periodic states or spatio-temporal patterns are considered, where an analytical discussion of the corresponding Floquet problem seems to be at the moment out of reach. However, some insight can be gained by numerical results and the semiquantitative discussion presented above.

We have focussed here on the simplest type of spatio-temporal patterns which admit just a single unstable mode. Whether time–delayed feedback methods can be applied successfully to fully developed extensive spatio–temporal chaos where numerous unstable modes are present remains still one of the challenges of spatio–temporal control of chaos (cf. e.g. [24]), from the experimental as well as from the theoretical point of view.

This work was partially supported by Deutsche Forschungsgemeinschaft in the framework of Sfb 555 and by the National Science Foundation through grant PHY-98-70028.

---

[1] H. G. Schuster, *Handbook of chaos control* (Wiley-VCH, Weinheim, 1999).
[2] H. Nijmeijer and A. J. van der Schaft, *Nonlinear Dynamical Control Systems* (Springer, New York, 1996)
[3] E. Ott, C. Grebogi, and J. A. Yorke, Phys. Rev. Lett. **64**, 1196 (1990).
[4] K. Pyragas, Phys. Lett. A **170**, 421 (1992).
[5] S. Bielawski, D. Derozier, and P. Glorieux, Phys. Rev. E **49**, R971 (1994).
[6] T. Pierre, G. Bonhomme, and A. Atipo, Phys. Rev. Lett. **76**, 2290 (1996).
[7] W. Just, T. Bernard, M. Ostheimer, E. Reibold, and H. Benner, Phys. Rev. Lett. **78**, 203 (1997).
[8] H. Nakajima, Phys. Lett. A **232**, 207 (1997).
[9] M. E. Bleich and J. E. S. Socolar, Phys. Lett. A **210**, 87 (1996).
[10] G. Franceschini, S. Bose, and E. Schöll, Phys. Rev. E **60**, 5426 (1999).
[11] E. Schöll, *Nonlinear spatio-temporal dynamics and chaos in semiconductors* (Cambridge University Press, Cambridge, 2001).
[12] F. Plenge, P. Rodin, E. Schöll, and K. Krischer, Phys. Rev. E **64**, 056229 (2001).
[13] A. Wacker and E. Schöll, Z. Phys. B **93**, 431 (1994).
[14] S. Bose, A. Wacker, and E. Schöll, Phys. Lett. A **195**, 144 (1994).
[15] M. Meixner, P. Rodin, E. Schöll, and A. Wacker, Eur. Phys. J. B **13**, 157 (2000).
[16] S. Bose, P. Rodin, and E. Schöll, Phys. Rev. E **62**, 1778 (2000).
[17] A. Alekseev, S. Bose, P. Rodin and E. Schöll, Phys. Rev. E **57**, 2640 (1998).
[18] J. E. S. Socolar, D. W. Sukow, and D. J. Gauthier, Phys. Rev. E **50**, 3245 (1994).
[19] K. Pyragas, Phys. Rev. Lett. **86**, 2265 (2001).
[20] W. Just, E. Reibold, H. Benner, K. Kacperski, P. Fronczak, and J. Holyst, Phys. Lett. A **254**, 158 (1999).
[21] W. Just, E. Reibold, K. Kacperski, P. Fronczak, J. A. Holyst, and H. Benner, Phys. Rev. E **61**, 5045 (2000).
[22] G. Benettin, L. Galgani, A. Giorgilli, and J. Strelcyn, Meccanica **15**, 9&21 (1980).
[23] J. K. Hale and S. M. V. Lunel, *Introduction to Functional Differential Equations* (Springer, New York, 1993).
[24] M. E. Bleich, D. Hochheiser, J. V. Moloney, and J. E. S. Socolar, Phys. Rev. E **55**, 2119 (1997).